JP Journal of Heat and Mass Transfer

http://www.pphmj.com
http://dx.doi.org/10.17654/HM014020247
Volume 14, Number 2, 2017, Pages 247-275 **ISSN: 0973-5763**

MOISTURE CONTENT ESTIMATION BASED ON A THERMAL ANALYSIS METHOD APPLIED TO SAND

R. Derbal*, D. Defer, E. Antczak and F. Brachelet

Laboratoire de Génie Civil et géo-Environnement (LGCgE)
Faculté des Sciences Appliquées
Université d'Artois
Technoparc Futura
62400 Béthune, France

Abstract

This paper presents a thermal analysis method based on inverse heat transfer to estimate moisture content. The inverse method is based on numerical and experimental studies. A sand multilayer at different moisture contents is thermally excited. Thermocouple probes are placed at different depths within the sand and at the extremities of the multilayer where temperature variations were recorded during the experiment. Prior test results are model inputs and provide empirical relationships between the thermophysical properties and the moisture content. A numerical heat transfer model based on finite difference approach associated with a Levenberg-Marquardt optimization algorithm allows layers' moisture contents estimation.

Received: July 1, 2016; Revised: September 25, 2016; Accepted: October 17, 2016
Keywords and phrases: moisture content, inverse heat transfer, thermal characterization, thermophysical properties.

*Corresponding author

Communicated by Abderrahmane Bairi

List of Symbols

C	Specific heat capacity $JK^{-1}kg^{-1}$
S	Sensitivity
F	Objective function
W'	Estimated moisture content set %
f	Weighted residuals
m	Mass kg
p	Parameters array
T	Temperature °C
t	Time s
x	Space (thickness) m

Greek Letters

Δt	Time-step s
Δx	Space-step m
$\Delta\omega$	Absolute error on moisture content %
α	Thermal diffusivity m^2s^{-1}
ε	Minimum user defined value
φ	Heat flux density Wm^{-2}
λ	Thermal conductivity $WK^{-1}m^{-1}$
λ_A	LMA damping factor
ρ	Density kgm^{-3}
ρC	Volumetric heat capacity $JK^{-1}m^{-3}$

ρ_{dry}	Dry density kgm^{-3}
ω	Moisture content %
ω_{sat}	Saturated moisture content %

Subscripts

b	Bottom
cal	Calculated
i	Time index
ini or 0	Initial
j	Space index
m	Middle layer position index
meas	Measured
ref	Reference
sim	Simulated
u	Upper

1. Introduction

Measuring moisture content is crucial with any soil processes. In the geothermal area, an optimal heat transfer between the medium and the buried collectors, like ground source heat pumps (GSHPs) or borehole heat exchangers (BHEs), is necessary, to exploit the efficiently renewable energy of soil [1-5].

In ground heat pump applications, deposition or extraction of thermal energy from the ground is accomplished by using a ground heat exchanger (GHE) [6], whose operation induces simultaneous heat and moisture flow in the surrounding soil. Thus, the energy efficiency of buried systems is directly related to the soil properties including its layers and also to moisture content,

which impacts the heat transfer. Therefore, thorough knowledge of the intricate nature of soils related to coupled heat and moisture in the ground is essential to both the design and operation of ground heat pump systems. Recent papers dealing with the influence of soil moisture conditions on ground heat pump performance have been published [7-9]. It was found that the soil moisture content was a dominant factor responsible for seasonal thermal conductivity variations. The effect of soil conditions and thermal conductivity on heat transfer in ground heat storage was also demonstrated. That is why, it is necessary to know not only the thermal properties for the use of heat pumps from the ground, but also to measure ground water content. As the thermal properties and water content of a soil are closely related, it makes sense to study one by the other.

In different other fields, studies highlight the relation between moisture content and heat transfer [10-14]. For optimal exploitation of the studied systems, one should capture the media moisture distribution.

Several methods are available to measure moisture content [15]. Time domain reflectometry is an available in situ method, as also is time domain transmissometry. They are studied and discussed; their limits are mainly due to their sensitivity to the soil salinity, calibration, and operator [16, 17]. The neutron probe method is also an available method. Its limits are mainly due to the high price and high risk [18]. Other methods, like ground penetrating radar, tensiometers, or remote sensing, allow moisture content determination or monitoring [19-21].

In addition to the cited methods, interesting thermal analysis based methods exist. The dual (or multi) thermal probe is basically used to measure the thermal properties (hot wire method) of a material, but has been adapted to measure soil moisture content [22, 23]. The major interest of the method is its ability to measure the moisture content near the surface. The method disadvantages are the same as for the hot wire method. The measurement uncertainties are mainly due to the wire dimensions or thermal inertia [24]. The thermo-TDR combines a heat pulse sensor (a thermal probe and a heat

source) and a classic TDR. The advantage of this method is its ability to measure more than one parameter at the same time. Thus, it was used to measure soil water flux and pore water velocity [25]. As it combines the two cited methods, this method also combines their disadvantages, such as sensor dimensions and high soil salinity dependence. Other field methods rely on thermal inertia to estimate the moisture content near the surface of bare soil [26]. However, if the sensing is expensive, the method will be onerous, cumbersome or not easy to use.

The actual work is based on inverse heat transfer analysis. A numerical study has been performed (Section 2) before any experimental work (Section 3). The study considers a multilayered homogeneous configuration of the tested soil (sand). Four separated layers at different moisture contents are considered (Figure 1). They represent the vertical moisture content variation in the multilayer. The moisture content noted below $\omega\,(\%)$ or p, is imposed constant parameter vertically and horizontally in each layer. This assumption is discussed in the experimental part (Section 3). Prior tests are performed to determine relationship between the sands' thermophysical properties $(\lambda(W/m/K)$: thermal conductivity and $\rho C(J/K/\mathrm{m}^3)$: volumetric heat capacity) and its moisture content $\omega\,(\%)$. The actual method aims to estimate the four mean moisture contents of the multilayer. It is based on the temperature measurement at different positions during a test (Figure 1). The theoretical and numerical studies are based on the heat transfer equation and the finite difference method associated to the Levenberg-Marquardt Algorithm (LMA): optimization algorithm. Their usual assumptions are discussed later in Section 2. On one hand, the method uses a simple experimental setup. On the other hand, it considers the only heat transfer to estimate a mass transfer parameter. This makes the method easy to use, not expensive and non-intrusive due to the thermocouples small dimension. These are the major interesting points of the method. The method can be useful in several application areas.

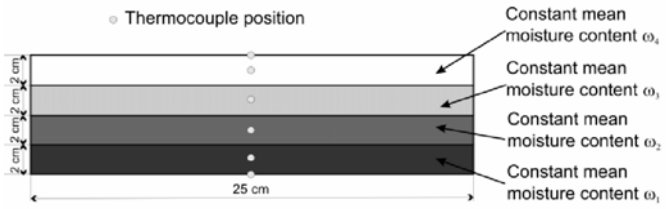

Figure 1. Sample tested in a multilayered configuration.

2. Numerical Study

2.1. Numerical model

Heat transfer occurs only through unidirectional conduction, without heat generation. This is due to the fact that the medium is supposed as solid, homogeneous and non-transparent. This is also due to the establishment of the experimental process, when for example, transversal sample's dimensions are greater than its thickness, or probes selected locations that allows to avoid edge effects (refer to Figures 1 and 2, and Subsection 3.2). Note that in other studies higher dimensions were considered for materials characterization [27]. In this case (1-D), the heat transfer is determined by the heat conduction equation (equation (1)). One can connect it to equations (6) and (7) (refer to Subsection 3.1). Its numerical solution is described later. It is based on the finite difference method suitable for our case study [28]

$$\frac{\partial T}{\partial t} = \frac{\lambda(\omega)}{\rho C(\omega)} \frac{\partial^2 T}{\partial x^2}. \tag{1}$$

A multilayered horizontal material is studied (for the case of in situ media - soils). The finite difference spatiotemporal discretization is applied to the multilayer. The successive four layers are discretized along the thickness into M nodes $(j = 0, 1, ..., M)$. The space step between two nodes is Δx. The total test time is discretized into N intervals $(i = 0, 1, ..., N)$. The time step is $\Delta t = 4\text{s}$, which is also the temperature recording time step during an experimental test. The heat transfer is unidirectional with no lateral loss (more details in Subsection 3.2) through the thickness of the multilayer,

where temperature evolution is simulated, after solving equation (1). 1-D transfer was also confirmed by measuring soil temperature at positions other than the middle of the soil layer.

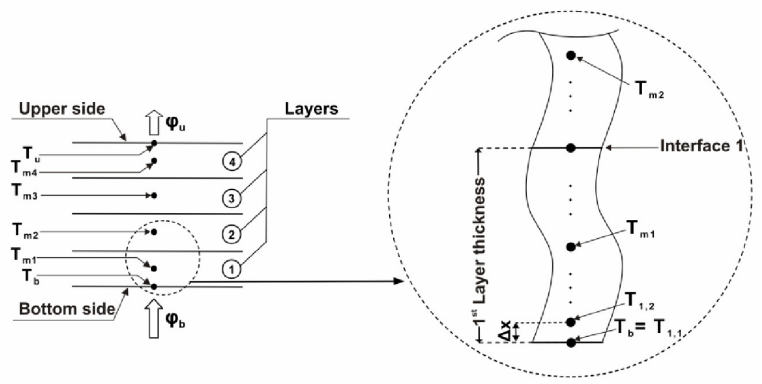

Figure 2. Tested multilayer and discretization details.

Numerically, we introduce the known initial condition, which is a one column matrix: $T_{ini}(j\Delta x)$. This is the initial temperature field through the multilayer thickness, carefully defined from initial recorded temperatures and noted T_{ini}. We also introduce the known two boundary conditions. Each boundary condition is a one column matrix representing the temperature field at the top: $T_u = T_u(i\Delta t)$, and at the bottom of the multilayer: $T_b = T_b(i\Delta t)$. These Dirichlet boundary conditions make it possible not to have to rely on the determination of the convection and radiation coefficient. The matrix system of the finite difference method applied on the conductive heat transfer depends on the thermophysical properties and dimensions of the sample (four layers). Thus, it depends on the moisture content (four moisture contents corresponding to each layer). Matlab® is used to solve the described numerical model, and thus provides all the simulated temperatures. Throughout the actual study, we are interested in the simulated temperatures in the middle of each layer (Figure 2): $(T_{sim}(m1, i\Delta t),\ T_{sim}(m2, i\Delta t),\ T_{sim}(m3, i\Delta t),\ T_{sim}(m4, i\Delta t),\ where:\ i = 1, ..., N)$. For simplification, they are noted T_{sim1}, T_{sim2}, T_{sim3} and T_{sim4}, simultaneously.

The location nodes $m1$, $m2$, $m3$ and $m4$ correspond to the nodes where the temperature fields are recorded during a test (Subsection 3.2): T_{meas1}, T_{meas2}, T_{meas3} and T_{meas4}. Continuity at the interfaces is assumed to be established. A thin waterproof film placed between layers has a negligible thickness $(12\mu m)$. Thus, their thermal resistance and heat capacity do not affect the conductive heat transfer [29]. Particular attention is paid when placing the films, so that additional contact resistances are avoided and numerical assumption respected.

The results of the developed numerical model (simulated temperatures) based on the finite difference method and the results of experimental tests (measured temperatures) are both associated in a parametric estimation algorithm. This allows moisture content estimation of every layer, by fitting the simulated temperatures to the measured ones.

Thereafter, the parametric estimation method is described. The connection is made between the numerical model and the parametric estimation. The whole numerical process is explained.

2.2. Parametric estimation

In this study, we used the Levenberg-Marquardt algorithm (LMA). This was first introduced by Levenberg [30], and developed by Marquardt [31]. It is still being improved and adapted, in recent studies [32]. This algorithm has now become a standard that has always provided good results in the actual conditions.

The connection between the experimental results, the finite difference numerical model, and the LMA leads to an inverse analysis model. The initial parameter set "p_0" is a vector of four mean moisture content values (i.e., between 5% and 31.7%, please refer to Subsection 3.1). Numerically, other tested initial parameters provide similar results. Thermal properties are calculated from the parameter set "p" thanks to equations (6) and (7). This allows to the numerical model to solve the heat equation (equation (1)) and to simulate temperature through the medium thickness. Then the LMA compares them to the measured temperatures, and tries at each step to

minimize an objective function that we defined, noted *F*. In this work, the objective function *F* set from a weighted least square is defined by the following equations (2) and (3). This uses the four simulated and measured temperature vector differences $(T_{meas\ j} - T_{sim\ j},\ j = 1, ..., 4)$. The LMA checks for the stopping criteria and then it either proposes another parameter set, or displays the last one found. Details about the algorithm are not discussed here. For more information, please refer to previous work [33]. Figure 3 below presents an inversion analysis diagram:

$$f_j(p) = \frac{T_{meas\ j} - T_{sim\ j}(p)}{\max(T_{meas\ j}) - \min(T_{meas\ j})}, \tag{2}$$

$$F(p) = \sum_j (f_j(p))^2, \tag{3}$$

where: $j = 1, ..., 4$ $(nodes\ m1, ..., m4)$ and p: vector of parameters to estimate (moisture content of each layer ω_j).

In fact, the LMA is a descent method and uses both Jacobian and Hessian. Elements of the derivative used in calculation are sensitive parameters on which depends the choice of the descent direction and the damping factor. Hereafter, the algorithm is explained step by step:

(1) Choose parameters initial values and an initial damping factor (λ_A generally equals to 10^4); iteration 1 starts $(i = 1)$.

(2) Calculate the Jacobian (iteration *i*).

(3) Check the current parameters (p_i) optimality (all sensitive elements are lower than a user defined value): Y/N = stop/continue.

(4) Find new parameters $p_{i+1} = p_i + h_{LMA}$ (this last is the descent direction).

(5) Compare $F(p_{i+1})$ to $F(p_i)$ and then calculate the new damping factor. If $F(p_{i+1}) - F(p_i) < 0$, then choose a lower λ_A and go to step 2 else choose a higher λ_A and go to Step 4.

At the end of the calculation, the algorithm outputs the last parameters set (four estimated moisture contents, one for each layer of the sample), as well as the simulated and measured temperature fields. The graphs offer information about the curve fitting and the objective function minimization.

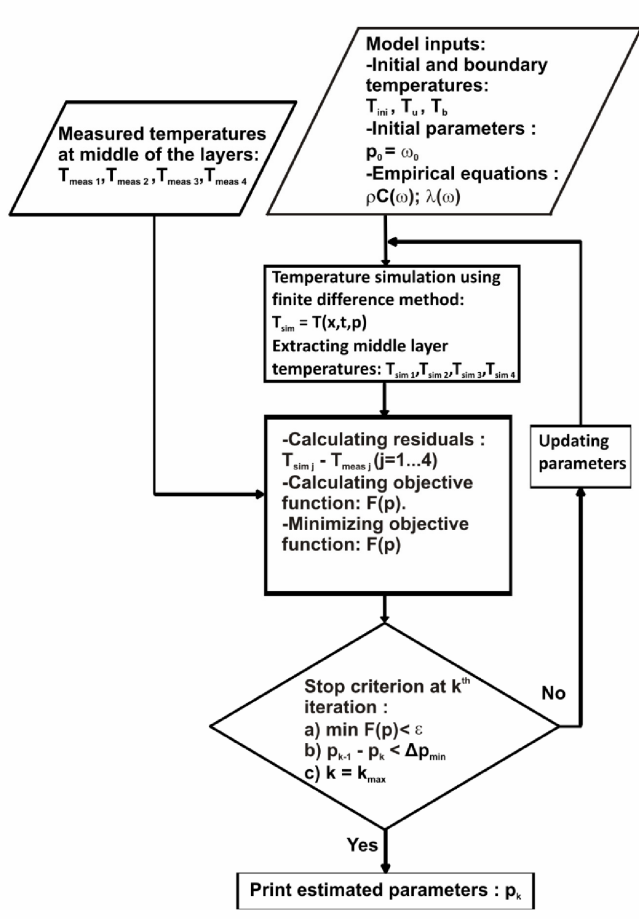

Figure 3. Inverse analysis diagram.

In this work, numerical tests with the developed numerical model, demonstrate that empirical relationships (equations (6) and (7): refer to Subsection 3.1) [29] provide more precise results in comparison with the previous studies results [34, 35]. This comes from the fact that in the actual study, we used exactly the same material used by Chauchois while Kersten

established equations for ranges of soils. Concerning the specific heat, there is a significant similarity between the previous work results of Chauchois and Laurent [29, 35]. Using their results, we obtain the empirical relationships between the volumetric heat capacity and the moisture content. Therefore, equations (6) and (7) are used to represent the thermal behavior according to the moisture content.

From then on, we exploit the inverse heat transfer analysis for moisture content estimation to carry out a sensitivity study. This provides information about the reliability of the developed process and its settings, like the minimum necessary test time, or minimum valuable parameters. Subsection 2.3 develops valuable information to take into account before the experimental work. The approach uncertainty on moisture content estimation is possible in case of destructive tests like in the actual study. However, when using the actual approach for non-destructive in situ tests, the uncertainty on estimation cannot be quantified.

2.3. Sensitivity study

In this work, a sensitivity study was numerically achieved, before starting the experimental part. This study focuses on the impact of a parameter, one among the four moisture contents to be estimated, variation on the simulated temperatures. If a parameter variation induces slight variations in the simulated temperatures, then this implies that the model is relatively insensitive to tested parameter. So its estimation will be difficult. In addition, this study provides an optimal test time for which a satisfying numerical model's sensitivity is obtained as well as simultaneous parameters identification. It is also necessary for the optimal test time window to have LMA valuable inputs (temperatures) and good parameter estimation (moisture contents of the four layers).

To carry out the actual sensitivity study, we consider a simple problem. In fact, the initial constant temperature is imposed through the material: $T_{ini} = 20°C$. Boundary conditions arise from instant t_0, which remains

constant during the test: $T_u = 20°C$, $T_b = 23°C$. Other initial and boundary conditions were tested and similar results were found. From the bottom to the top, the moisture contents of the tested layers are: $\omega_1 = 20\%$, $\omega_2 = 15\%$, $\omega_3 = 10\%$ and $\omega_4 = 5\%$. These moisture content variations from one layer to another give rise to variation in thermophysical properties (refer to equations (6) and (7)). After the first 1800 time steps, a steady state is established. This corresponds to the useful time window (7200 seconds).

The sensitivity is expressed as follows (equation (4)):

$$S_{\omega_j}(t) = \Delta T(t) / \left(\frac{\Delta \omega_j}{\omega_j} \right), \tag{4}$$

where $j = 1, ..., 4$ (corresponds to the four layers).

The derivative is numerically calculated by varying the parameter ω_j around its nominal value. The graphs in Figures 4.1 to 4.4 represent the temperature sensitivity functions in relation to the tested parameters ω_j.

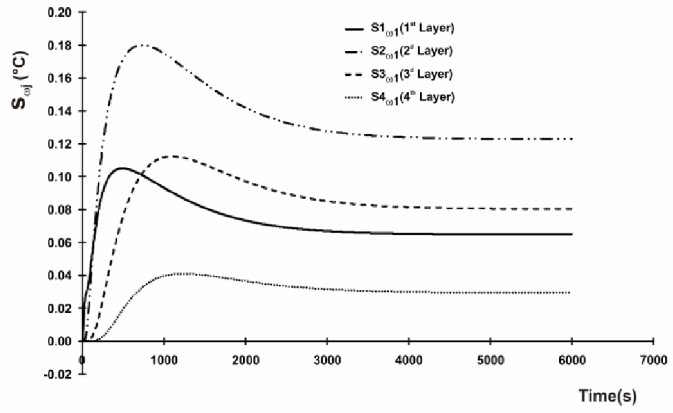

Figure 4.1. Numerical model sensitivity in relation to ω_1 in positions *m*1, *m*2, *m*3 and *m*4.

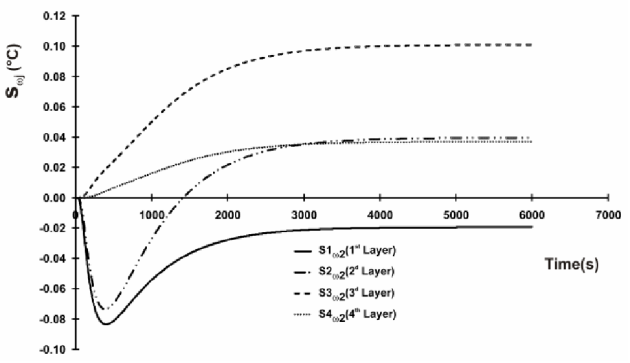

Figure 4.2. Numerical model sensitivity in relation to ω_2 in positions *m*1, *m*2, *m*3 and *m*4.

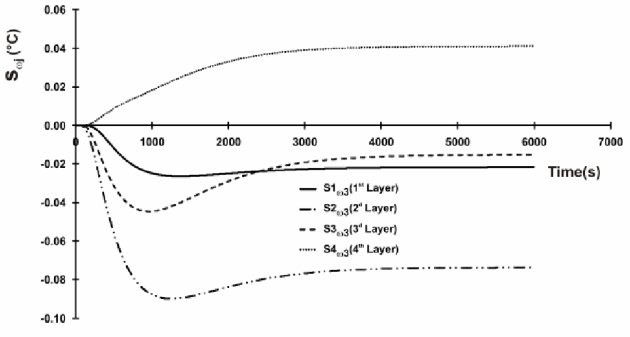

Figure 4.3. Numerical model sensitivity in relation to ω_3 in positions *m*1, *m*2, *m*3 and *m*4.

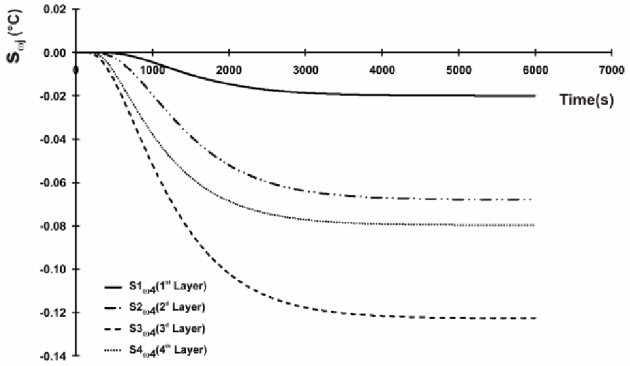

Figure 4.4. Numerical model sensitivity in relation to ω_4 in positions *m*1, *m*2, *m*3 and *m*4.

The downstream and upstream temperature fields of a considered layer are impacted by the imposed variations on moisture content. The effect decreases with the distance. The nearest nodes to heat or moisture content variations are the most sensitive. The distant nodes undergo less variation than the first ones. For the actual considered heat excitation, the graphs show that the steady state is almost reached in 6000 seconds. The sensitivity curves are then all parallel to the *x*-coordinate. After this time window, no more additional relevant information is provided. In the first part of the test (i.e., from 0 to 2000s), the sensitivity curves behave differently, and suggest non-significant correlation between the parameters to be estimated. After this (i.e., from 2000 to 6000s), the sensitivity curves tend to be proportional. This part of the test is used to consolidate the parameter estimation, because the temperature changes are related to the parameters, relationships.

A statistical approach is used to test the correlation between parameters. Thus, uncorrelated and randomly normally-distributed variables are defined around moisture content reference values of the four layers (i.e., 20%, 15%, 10% and 5%). These variables are noted $W = (\omega_1\omega_2\omega_3\omega_4)^t$. Temperatures were simulated for each vector *W*, using the same initial and boundary conditions. An inverse process using these simulated temperatures allows parameter estimation. The estimated parameters are noted $W' = (\omega'_1\omega'_2\omega'_3\omega'_4)^t$. The covariance matrix of W' is calculated (equation (5)). Parameter correlation is discussed. This is based on matrix elements comparative study

$$COV(W') = 10^{-3}\begin{pmatrix} 108.53 & 9.87 & 0.04 & 0.63 \\ 9.87 & 98.24 & 3.77 & -1.13 \\ 0.04 & 3.77 & 4.94 & -0.23 \\ 0.63 & -1.13 & -0.23 & 1.13 \end{pmatrix}. \quad (5)$$

From equation (5), one can note that the covariance matrix is positive-definite (positive eigenvalues). This means that no notable linear relationship

exists between the estimated parameters. The relatively low values of the non-diagonal covariance matrix elements support this conclusion. The sensitivity study has demonstrated that the developed model is sensitive to all parameters, and the method allows simultaneous parameters estimation. The parameters are the four layers non-correlated moisture contents. It also has demonstrated that at least the first 1500 iterations are needed to perform a correct test. This corresponds to a minimum test time of 6000s.

Temperature measurement noise can influence on the estimation. Thus, a temperature standard deviation of 0.04°C due to a normal distributed noise is taken into account to make three series of 100 numerical tests. The moisture content maximum standard deviation on the four parameters $(\omega_{j,\ j=1,\ldots,4})$ is equal to 0.23%. Thus, for calibrated thermocouples (+/-0.1°C), fluctuation temperature can lead to a maximum deviation of 0.7% on moisture content estimation. One can see that the reasonable but real supposed noise on temperature does not affect significantly the parameters' estimation.

Sensors placement, layers load and setup movement can lead to positioning errors determined to be +/-1mm maximum (+/-5% in terms of relative error). One can note that for larger dimensions this relative error is lower and consequently estimation errors too. To define the influence of these errors on parameters' estimation, a simulation has been made under a temperature gradient for different cases. The results are summarized in Table 1. One can see that the error on thermocouple positioning is amplified by the fact that its position is near from the heat source (multilayer bottom where T_b = 23°C). This is confirmed by the high relative errors on the first moisture content ω_1 due to positioning error at the middle of the first layer. This study shows that a maximum uncertainty of 0.51% on moisture content estimation due to thermocouple positioning has to be considered.

Table 1. Estimation errors due to the thermocouples positioning error

Layer number	Error on thermocouple position (mm)	Relative error on $\omega_1(\%)$	Relative error on $\omega_2(\%)$	Relative error on $\omega_3(\%)$	Relative error on $\omega_4(\%)$	Maximum absolute error (%)
1	+1.00	4.56	1.81	1.56	0.81	0.23
1	-1.00	5.43	1.94	1.43	1.02	0.27
2	+1.00	1.37	3.59	1.61	1.22	0.36
2	-1.00	1.52	4.78	2.12	1.30	0.48
3	+1.00	1.09	1.99	2.59	1.52	0.39
3	-1.00	1.02	2.18	3.02	1.74	0.45
4	+1.00	0.95	1.22	2.01	2.55	0.51
4	-1.00	1.03	1.51	2.08	2.56	0.51

3. Experimental Setup

3.1. Material prior characterization

The moisture content obviously influences the heat transfer through a granular medium. It directly impacts the thermophysical properties of soils [29, 36-41]. The devising of a method capable of linking the thermophysical quantities of the soil to its water content is therefore important, since these parameters appear to be closely interconnected.

Relationships between the tested sand water content $(\omega(\%))$ and its thermophysical properties ($\lambda(\mathrm{W/m/K})$: thermal conductivity and $\rho C(\mathrm{J/K/m^3})$: volumetric heat capacity) were established in previous works in our laboratory, and are used in this study [29] (equation (6) and equation (7) defined for moisture contents greater than 5%). These empirical relationships are comparable to those cited in the literature [34, 35] (refer to Table 2)

$$\rho C(\omega) = -269.13 \cdot \omega^2 + 35.25 \cdot 10^3 \cdot \omega + 130.67 \cdot 10^4, \quad (6)$$

$$\lambda(\omega) = -8 \cdot 10^{-4} \cdot \omega^2 + 6.84 \cdot 10^{-2} \cdot \omega + 8.82 \cdot 10^{-2}. \quad (7)$$

Table 2. Thermophysical properties related to moisture content

ω (%)	0.00(dry)	05.0	10.0	15.0	20.0	25.0	31.7(saturated)
λ_Chauchois (W/K/m)	0.25	1.20	1.50	1.70	1.90	2.10	2.20
λ_Kersten (W/K/m)	N/A	1.23	1.56	1.76	1.89	2.00	2.12
C_Chauchois (J/K/kg)	737	929	1058	1152	1249	1402	1593
C_Laurent (J/K/kg)	770	898	1026	1154	1282	1409	1581

Table 3 and Figure 5 show some characteristics of the used sand.

Table 3. Sand properties

Fine sand	Fineness modulus (M_f)	Dry density $(\gamma_d)(\mathrm{kg/m^3})$	Moisture content at saturation $(\omega_{sat})(\%)$
(0/0.45)	1.2	1700	31.7

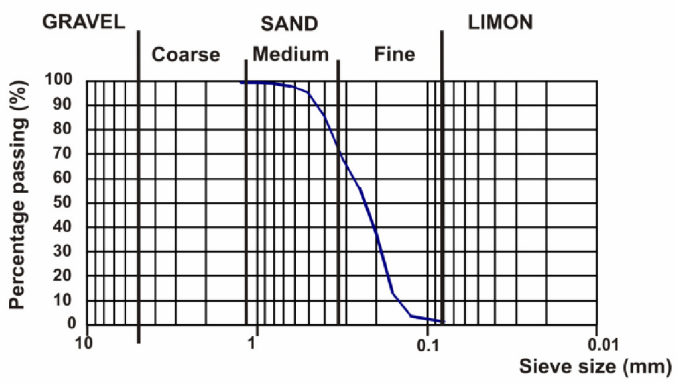

Figure 5. Sieve analysis graph of the tested material (fine sand).

3.2. Experimental tests

The experimental instrumentation consists of a tested multilayered material equipped with thermocouples, a flat heating resistance, a cold junction terminal block for differential measures, a data logger, and a control computer (Figure 6.1).

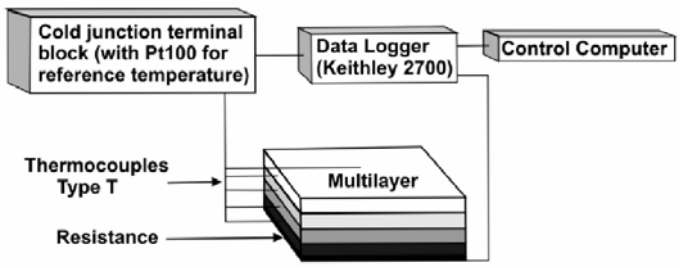

Figure 6.1. Experimental setup.

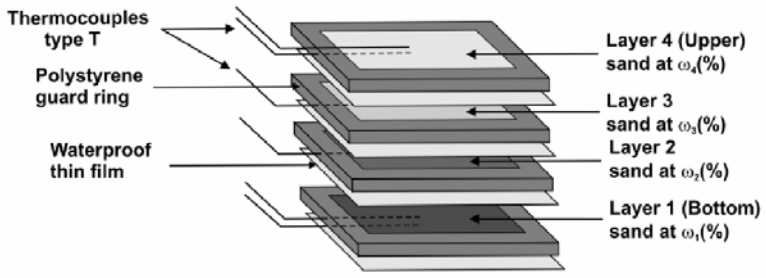

Figure 6.2. Tested multilayer details.

The multilayer is made of four thin layers of sand (2cm thickness) separated by a thin (12µm thickness) waterproof film. Layers placed horizontally are at different moisture contents $(\omega_1, \omega_2, \omega_3, \omega_4) \approx (20\%, 15\%, 10\%, 5\%)$. These different moisture contents are achieved by wetting and mixing dry sand (stable weight reached after 7 days in an oven at 105°C), after adding different amounts of water. The different moisture contents were defined by mean of a gravimetric method using a 0.1g precision balance. During the sample preparation, the mean absolute error due to weighing and positioning is up to 0.5% (assumed after increasing the cumulated errors of balance, moisture loss after a test and supposed setup movements). The layers are arranged in decreasing order of moisture content, from the bottom to the top. Each layer is inserted in a 2cm thickness polystyrene guard ring. This maintains sand, and limits lateral heat losses. Thus, a unidirectional heat transfer is guaranteed. Introduction of the sand in its guard ring is made in two parts. The first one is to fill in the first centimeter layer thickness without compaction on the whole surface

$(25 \times 25\text{cm}^2)$. The thermocouple is inserted in the middle of the layer. After that, the second centimeter layer thickness is filled, following exactly the same procedure as the first centimeter, with the same material and the same moisture content. This ensures correct positioning of the thermocouple centered in the middle of the layer volume $(25 \times 25 \times 2\text{cm}^3)$. The same process is repeated for the three other layers. *T*-type thermocouples allow the temperature field to be recorded at the middle of each layer (T_{meas1}, T_{meas2}, T_{meas3} and T_{meas4}). A thin (12µm thickness) waterproof film is placed at the layers' interfaces. This prevents layer water exchanges and losses, either liquid or vapor. Thus, it enables an established heat transfer, and a limited mass transfer. Table 4 shows the layer mass evolution during a 12-hour test. This is the maximum test time to prevent likely mass transfer occurring even under low temperature gradient of 3°C. The weight loss and moisture content deviation low values allow us to consider layers' constant mean moisture contents. A thin film also separates the bottom layer, and the heating resistance $(25 \times 25\text{cm}^2, 19.2\Omega)$. The upper layer is in direct contact with the ambient air. These two last boundaries are equipped with *T*-type thermocouples in the middle surface at the top and the bottom. They allow us to record temperature fields at the extremities (boundary conditions: T_u and T_b) (Figure 6.2). The heating resistance is placed under all layers of the tested sample and on an insulating base, which directs the main heat flow dissipated by the resistance to the top, in the direction of the multilayer. This base consists of a Polyurethane plate (5cm thickness) and PVC plate (1cm thickness), which offers a flat surface to the setup establishment. This experimental setup configuration (polystyrene guard ring, thin waterproof film, and heat source dimension equal to those of the samples …) allows a unidirectional heat transfer. This was inspired by several standards, like ASTM C 1363-05 and ISO 8990.

The thermocouples are non-insulated junction type T: copper/constantan (0.08×2mm diameter or 2×40 American wire gauge); Class 1 referring to EN 60584-2 with a tolerance of +/-0.5°C within the temperature range-40 to

125°C. The thermocouples' temperatures observed deviations were inferior to 0.1°C compared to a calibrated thermometer (Pt100 WIKACTH 6500 0.03°C precision probe). They are connected to a cold junction terminal block. A Pt100 resistance thermometer is also connected to the block, to provide a reference experimental temperature, which is necessary for differential measurement. The purpose of using a differential measurement terminal block is to overcome possible temperature fluctuations at the data logger card.

The data logger is a multimeter scanner (Keithley 2700) fitted with a multiplexing card for measuring, and with two voltage output dedicated channels. One of the two channels stimulates the heating resistance via a power amplifier. The scan time is the same as time step used in the numerical study which is equal to 4 seconds for all performed tests.

A computer interface allows communication with the data logger and the power amplifier. It stores and prints the acquired data.

Table 4. Layers mass evolution during one of 12 hour tests at different moisture contents

Mean moisture content values (%)	5	10	15	20
Mass before test (g)	5312.4	5485.2	5750.1	6037.5
Mass after test (g)	5308.1	5479.1	5735.3	6017.4
Weight loss (%)	0.07	0.11	0.26	0.33
Absolute moisture content deviation (%)	0.08	0.03	0.03	0.04

The six measured temperature fields (T_u, T_{meas1}, T_{meas2}, T_{meas3}, T_{meas4} and T_b) during a test are numerically exploited. The next section presents and discusses the results.

4. Results and Discussion

The numerical study associated with the experimental procedure leads to an inverse heat transfer analysis. This section presents and discusses the results of the whole process.

Previous studies allow us to define the relationships between the thermophysical properties ($\lambda(\mathrm{W/m/K})$: thermal conductivity and $\rho C(\mathrm{J/K/m^3})$: volumetric heat capacity) and moisture content: $\omega(\%)$. These results (equations (6) and (7)) were used in the current study. It is worth recalling that these relationships are only valid for $\omega \geq 5\%$. These empirical relationships were introduced in the inverse heat transfer analysis. This allows the parametric estimation to deal with the four moisture contents of the tested layers, and not directly with their eight thermophysical properties. Thus, the optimization is improved, and the estimation errors are reduced.

A test campaign is a series of tests conducted on a sample using the experimental setup. In the campaign, four distinct tests were performed. The sample is a multilayer consisting of 4 layers at different mean constant moisture contents. From the bottom to the top: $\omega_1 \approx 20\%$, $\omega_2 \approx 15\%$, $\omega_3 \approx 10\%$ and $\omega_4 \approx 5\%$ $(\Delta\omega = \pm 0.5\%)$. The test campaign aims to record the temperature fields at the middle of each layer of the sample and also at its ends (boundaries). From the bottom to the top of the multilayer, the measured temperatures are: T_b, T_{meas1}, T_{meas2}, T_{meas3}, T_{meas4} and T_u. The thermal loads resulting from the flat heating resistance consist of randomly selected heat flux sequence levels. This allows the applicability of the device to be determined regardless of the excitation, and suggests in situ applications (Figure 7). The measurements are numerically exploited. This allows temperature simulation in the middle of each layer. Then the LMA operates for parameter estimation (the four layers' moisture contents: refer to Figure 3).

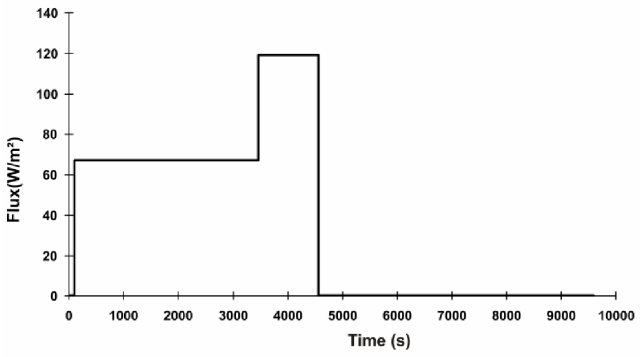

Figure 7. Heat flux delivered by the heating resistor during the presented test.

The following figures and tables summarize the test results. For clarity, the details of one test among others are presented in Figure 8. Tables 5 and 6 show the moisture content reference values (ω_{ref}), calculated moisture contents (ω_{cal}) and estimation errors.

Table 5. Results of one of the four tests: statistical indications about Figure 8

Position	*m*1	*m*2	*m*3	*m*4
$\mathrm{Max}(T_{sim}\text{-}T_{meas})$ $(10^{-2}\,°C)$	10.5	5.9	8.3	7.7
Standard deviation $(10^{-2}\,°C)$	2.2	1.1	1.7	1.7

Table 6. Results of one of the four tests: moisture content values and estimation errors

Test time (hours)	Layer number	ω_{ref} (%)	ω_{cal} (%)	Absolute error (%)	Relative error (%)
2.66	1(bottom)	20.00	20.28	0.28	1.41
	2	15.00	16.38	1.38	9.18
	3	10.00	11.00	1.00	10.02
	4(top)	5.00	5.08	0.08	1.66

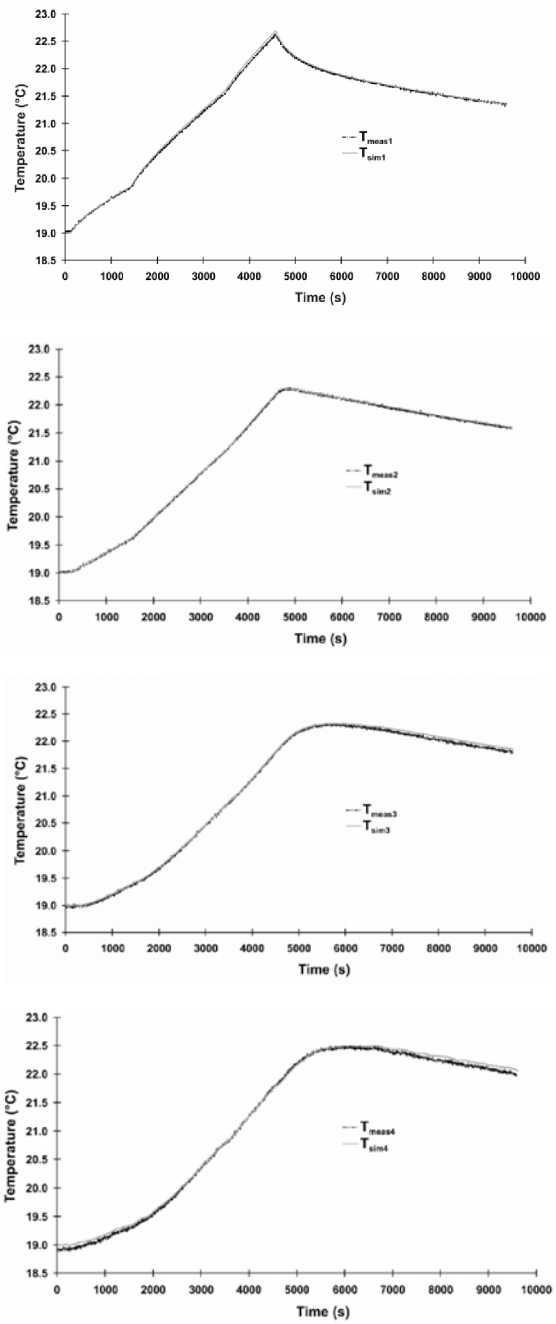

Figure 8. Results of one of the four tests: simulated after optimization and measured temperatures at the four nodes *m*1, *m*2, *m*3, *m*4.

For a good parametric estimation, we take into account a minimum value of the moisture content, and a good initial temperature representation. Sequence levels of thermal load delivered by the heating resistance are used. For information about the thermal load type, refer to Figure 7. The optimized time (6000s) is learned from the sensitivity study. Table 7 summarizes the tests series (4 tests were conducted, one after the other) results.

Table 7. Test results: mean values of the four tests

Position	ω_{ref} (%)	ω_{cal} (%)	Absolute error (%)	Relative error (%)
$m1$	20.00	20.37	0.37	1.86
$m2$	15.00	15.80	0.80	5.35
$m3$	10.00	10.40	0.40	4.00
$m4$	5.00	4.40	0.60	12.05

The presented results show a good parametric estimation, in light of the low relative error values. A good curve fitting is related to this parametric estimation. Table 7 shows that when the moisture content is close to or below the minimum moisture content threshold (5% at position $m4$), the empirical relationships (equations (6) and (7)) are no longer representative of the moisture content evolution related to the thermophysical properties. In this case, the estimation of this parameter is more difficult. Thus, it is estimated with high relative errors (> 12%). We consider the estimation on the whole tests campaign to be satisfactory. The well measured and simulated temperature curves fitting provide an appreciation of the objective function minimization.

Remember that errors on moisture contents estimation are possible to be determined in the actual work but in a non-destructive test this will not be possible or one must use another method for comparison. However, the worst scenario can be supposed in the actual study to cumulate all above analyzed errors: weighing and setup positioning (0.5%), temperature noise (0.7%), thermocouple positioning (0.51%), and maximum estimation error (1.38%). Thus, the maximum global absolute error on moisture content estimation in

the present case study case is 3.09%. This value is comparable to accurate moisture content instruments. An identical error analysis should be performed in other case studies.

5. Conclusion

The article presents a conductive thermal diffusion analysis for moisture content characterization. This method is applied here on fine sand, which is a homogeneous, stable, thermally reversible, and easy to use.

First, to apply the method, we needed prior tests to determine the relationship between the thermophysical properties (thermal conductivity and volumetric heat capacity) and water content of the sand. Then, by an inverse heat transfer analysis through the tested sample, we estimated the different moisture contents. This method is applied to a multilayer of 4 sand layers at different moisture contents (5%, 10%, 15% and 20%), separated by a thin waterproof film. The inversion algorithm implementation is based on a 1-D finite difference method. The algorithm exploits the temperatures measured by four thermocouples in the middle of each layer. The moisture contents were estimated with satisfactory relative errors of 1.86% to 5.35%. For the driest $(\omega_4 \approx 5\%)$, the mean relative error is higher (i.e., 12%). In this case, the correlation between thermophysical properties and moisture content reached its validity limit.

In this work, we consider watertight layers. The moisture content is supposed to be uniformly distributed in the thickness of each layer. We now plan to study a multilayer with continuously varying moisture content. To do this, we can include in the heat transfer simulation algorithm a function describing the spatial (1-D) variations of the moisture content. The aim is to deal with moisture content monitoring, and to reach an in situ stable application of the method.

Acknowledgement

The authors thank the anonymous referees for their constructive criticism and valuable suggestions.

References

[1] J.-Y. Lee and J.-S. Hahn, Characterization of groundwater temperature obtained from the Korean national groundwater monitoring stations: implications for heat pumps, Journal of Hydrology 329(3-4) (2006), 514-526.

[2] W. H. Leong, V. R. Tarnawski and A. Aittomäki, Effect of soil type and moisture content on ground heat pump performance: Effet du type et de l'humidité du sol sur la performance des pompes à chaleur à capteurs enterrés, International Journal of Refrigeration 21(8) (1998), 595-606.

[3] N. Molina-Giraldo, P. Bayer and P. Blum, Evaluating the influence of thermal dispersion on temperature plumes from geothermal systems using analytical solutions, International Journal of Thermal Sciences 50(7) (2011), 1223-1231.

[4] A. Mustafa Omer, Ground-source heat pumps systems and applications, Renewable and Sustainable Energy Reviews 12(2) (2008), 344-371.

[5] L. Lamarche, S. Kajl and B. Beauchamp, A review of methods to evaluate borehole thermal resistances in geothermal heat-pump systems, Geothermics 39(2) (2010), 187-200.

[6] C. Lee and S. Lee, An experimental study on the performance measurement of a heat pump using combined heat source heat exchange of fin-tube type, JP Journal of Heat and Mass Transfer 13(2) (2016), 229-238.

[7] N. Diao, Q. Li and Z. Fang, Heat transfer in ground heat exchangers with groundwater advection, International Journal of Thermal Sciences 43(12) (2004), 1203-1211.

[8] R. Garcia Gonzalez, A. Verhoef, P. L. Vidale, B. Main, G. Gan and Y. Wu, Interactions between the physical soil environment and a horizontal ground coupled heat pump, for a domestic site in the UK, Renewable Energy 44 (2012), 141-153.

[9] A. Hepbasli, Performance evaluation of a vertical ground-source heat pump system in Izmir, Turkey, International Journal of Energy Research 26(13) (2002), 1121-1139.

[10] A. Abdou and I. Budaiwi, The variation of thermal conductivity of fibrous insulation materials under different levels of moisture content, Construction and Building Materials 43 (2013), 533-544.

[11] E. Antczak, A. Chauchois, D. Defer and B. Duthoit, Characterisation of the thermal effusivity of a partially saturated soil by the inverse method in the frequency domain, Applied Thermal Engineering 23(12) (2003), 1525-1536.

[12] C. A. Chaves, J. R. Camargo, S. Cardoso and A. G. de Macedo, Transient natural convection heat transfer by double diffusion from a heated cylinder buried in a saturated porous medium, International Journal of Thermal Sciences 44(8) (2005), 720-725.

[13] R. de Lieto Vollaro, L. Fontana, A. Quintino and A. Vallati, Improving evaluation of the heat losses from arrays of pipes or electric cables buried in homogeneous soil, Applied Thermal Engineering 31(17-18) (2011), 3768-3773.

[14] Y. Dong and S. Pamukcu, Thermal and electrical conduction in unsaturated sand controlled by surface wettability, Acta Geotech. 10(6) (2014), 1-9.

[15] J. P. Walker, G. R. Willgoose and J. D. Kalma, In situ measurement of soil moisture: a comparison of techniques, Journal of Hydrology 293(1-4) (2004), 85-99.

[16] A. Bárdossy and W. Lehmann, Spatial distribution of soil moisture in a small catchment, Part 1: Geostatistical analysis, Journal of Hydrology 206(1-2) (1998), 1-15.

[17] R. Černý, Time-domain reflectometry method and its application for measuring moisture content in porous materials: a review, Measurement 42(3) (2009), 329-336.

[18] J. P. Bell, Neutron Probe Practice, 3rd ed., Institute of Hydrology, Wallingford, 1987, p. 51.

[19] P. Dobriyal, A. Qureshi, R. Badola and S. A. Hussain, A review of the methods available for estimating soil moisture and its implications for water resource management, Journal of Hydrology 458-459 (2012), 110-117.

[20] N. Romano, Soil moisture at local scale: measurements and simulations, Journal of Hydrology 516 (2014), 6-20.

[21] H. Vereecken, J. A. Huisman, Y. Pachepsky, C. Montzka J. van der Kruk, H. Bogena, L. Weihermüller, M. Herbst, G. Martinez and J. Vanderborght, On the spatio-temporal dynamics of soil moisture at the field scale, Journal of Hydrology 516 (2014), 76-96.

[22] K. L. Bristow, G. J. Kluitenberg, C. J. Goding and T. S. Fitzgerald, A small multi-needle probe for measuring soil thermal properties, water content and electrical conductivity, Computers and Electronics in Agriculture 31(3) (2001), 265-280.

[23] M. B. Kirkham, Chapter 9 - Dual Thermal Probes, M. B. Kirkham, ed., Principles of Soil and Plant Water Relations, 2nd ed., Academic Press, Boston, 2014, pp. 123-151.

[24] R. Coquard, D. Baillis and D. Quenard, Experimental and theoretical study of the hot-wire method applied to low-density thermal insulators, International Journal of Heat and Mass Transfer 49(23-24) (2006), 4511-4524.

[25] T. Ren, G. J. Kluitenberg and R. Horton, Determining Soil Water Flux and Pore Water Velocity by a Heat Pulse Technique, Soil Sci. Soc. Amer. J. 64(2) (2000), 552-560.

[26] M. Minacapilli, M. Iovino and F. Blanda, High resolution remote estimation of soil surface water content by a thermal inertia approach, Journal of Hydrology 379(3-4) (2009), 229-238.

[27] A. Baïri, J. M. García de María and N. Laraqi, Thermal diffusivity measurements of building materials based on 2D models, Computational Materials Science 38(4) (2007), 838-846.

[28] M. N. Özişik, Finite Difference Methods in Heat Transfer, CRC Press, Boca Raton, Fl, 1994.

[29] A. Chauchois, Modèles d'ordres non entiers appliqués à la caractérisation thermique de milieux évolutifs par méthode inverse: cas d'un sol humide, Béthune, 2002.

[30] K. Levenberg, A method for the solution of certain non-linear problems in least squares, Quart. Appl. Math. 2 (1944), 164-168.

[31] D. W. Marquardt, An algorithm for least-squares estimation of nonlinear parameters, Journal of the Society for Industrial and Applied Mathematics 11 (1953), 431-441.

[32] C. Kanzow, N. Yamashita and M. Fukushima, Levenberg-Marquardt Methods for Constrained Nonlinear Equations with Strong Local Convergence Properties, 2002.

[33] R. Derbal, D. Defer, A. Chauchois and E. Antczak, A simple method for building materials thermophysical properties estimation, Construction and Building Materials 63 (2014), 197-205.

[34] M. S. Kerstin, Thermal Properties of Soils, University of Minnesota, Minnesota, 1949.

[35] J. P. Laurent, Contribution à la caractérisation thermique des milieux poreux granulaires: optimisation d'outils de mesure "in-situ" des paramètres thermiques, application à l'étude des propriétés thermiques du matériau terre, Grenoble, 1986.

[36] M. Balghouthi, S. Kooli, A. Farhat, H. Daghari and A. Belghith, Experimental investigation of thermal and moisture behaviors of wet and dry soils with buried capillary heating system, Solar Energy 79(6) (2005), 669-681.

[37] O. T. Farouki, Thermal Properties of Soils, U. S. Army Cold Regions Research and Engineering Laboratory, Hanover, 1981, p. 151.

[38] M. Gangadhara Rao and D. N. Singh, A generalized relationship to estimate thermal resistivity of soils, Canadian Geotechnical Journal 36(4) (1999), 767-773.

[39] J. Lipiec, B. Usowicz and A. Ferrero, Impact of soil compaction and wetness on thermal properties of sloping vineyard soil, International Journal of Heat and Mass Transfer 50(19-20) (2007), 3837-3847.

[40] A. Kaemmerlen, F. Asllanaj, H. Sallée, D. Baillis and G. Jeandel, Transient modeling of combined conduction and radiation in wood fibre insulation and comparison with experimental data, International Journal of Thermal Sciences 49(11) (2010), 2169-2176.

[41] V. R. Tarnawski and W. H. Leong, Thermal conductivity of soils at very low moisture content and moderate temperatures, Transport in Porous Media 41(2) (2000), 137-147.